



The First Continuous Optical Monitoring of the Transitional Millisecond Pulsar PSR J1023+0038 with *Kepler*

A. Papitto¹ , N. Rea^{2,3,4} , F. Coti Zelati^{2,3}, D. de Martino⁵ , S. Scaringi⁶, S. Campana⁷ , E. de Oña Wilhelmi^{2,3}, C. Knigge⁸, A. Serenelli^{2,3} , L. Stella¹ , D. F. Torres^{2,3,9} , P. D’Avanzo⁷ , and G. L. Israel¹

¹INAF—Osservatorio Astronomico di Roma, via Frascati 33, I-00040, Monteporzio Catone (RM), Italy

²Institute of Space Sciences (ICE, CSIC), Campus UAB, Carrer de Can Magrans, E-08193, Barcelona, Spain

³Institut d’Estudis Espacials de Catalunya (IEEC), E-08034 Barcelona, Spain

⁴Anton Pannekoek Institute for Astronomy, University of Amsterdam, Postbus 94249, NL-1090-GE Amsterdam, The Netherlands

⁵INAF—Osservatorio Astronomico di Capodimonte, Salita Moiariello 16, I-80131 Napoli, Italy

⁶School of Physical and Chemical Sciences, University of Canterbury, Christchurch 8041, New Zealand

⁷INAF—Osservatorio Astronomico di Brera, via Bianchi 46, I-23807 Merate (LC), Italy

⁸Physics and Astronomy, University of Southampton, Highfield, Southampton SO17 1BJ, UK

⁹Institució Catalana de Recerca i Estudis Avançats (ICREA), E-08010 Barcelona, Spain

Received 2018 January 12; revised 2018 April 11; accepted 2018 April 12; published 2018 May 7

Abstract

We report on the first continuous, 80-day optical monitoring of the transitional millisecond pulsar PSR J1023+0038 carried out in mid 2017 with *Kepler* in the *K2* configuration, when an X-ray subluminescent accretion disk was present in the binary. Flares lasting from minutes to 14 hr were observed for 15.6% of the time, which is a larger fraction than previously reported on the basis of X-ray and past optical observations, and more frequently when the companion was at superior conjunction of the orbit. A sinusoidal modulation at the binary orbital period was also present with an amplitude of $\simeq 16\%$, which varied by a few percent over timescales of days, and with a maximum that took place 890 ± 85 s earlier than the superior conjunction of the donor. We interpret this phenomena in terms of reprocessing of the X-ray emission by an asymmetrically heated companion star surface and/or a non-axisymmetric outflow possibly launched close to the inner Lagrangian point. Furthermore, the non-flaring average emission varied by up to $\approx 40\%$ over a timescale of days in the absence of correspondingly large variations of the irradiating X-ray flux. The latter suggests that the observed changes in the average optical luminosity might be due to variations of the geometry, size, and/or mass accretion rate in the outer regions of the accretion disk.

Key words: pulsars: individual (PSR J1023+0038) – stars: neutron – X-rays: binaries

1. Introduction

Binary systems hosting a neutron star (NS) that accretes matter from a low-mass X-ray binary donor (NS-LMXB) are the progenitors of millisecond radio pulsars (MSP) powered by the rotation of the pulsar magnetic field. The link between MSPs and NS-LMXBs has been demonstrated by three transitional MSPs that switch between accretion and rotation-powered states on timescales of days/months due to variations of the mass inflow rate (PSR J1023+0038, Archibald et al. 2009; IGR J18245–2452, Papitto et al. 2013; XSS J12270–4859, de Martino et al. 2010; Bassa et al. 2014). In addition to accretion outbursts ($L_X = 10^{36-37}$ erg s⁻¹) and rotation-powered radio pulsar states ($L_X \approx 10^{32}$ erg s⁻¹), all three known transitional MSPs have been observed also in a peculiar X-ray subluminescent disk state ($L_X = 10^{33-34}$ erg s⁻¹).

Discovered as an eclipsing 1.69 ms radio pulsar in a 4.75 hr binary that previously had an accretion disk (Archibald et al. 2009), PSR J1023+0038 entered in a subluminescent disk state in 2013 June. The transition featured the appearance of a double-peaked H α emission line in the optical spectrum (Halpern et al. 2013), the disappearance of radio pulsations, and the increase of the X-ray and gamma-ray by a factor of about 10 and five, respectively (Patruno et al. 2014; Stappers et al. 2014; Tendulkar et al. 2014; Torres et al. 2017). The X-ray emission switches from a high mode ($L_X \sim 7 \times 10^{33}$ erg s⁻¹; 0.3–79 keV, 70%–80% of the time), to a low mode ($L_X \sim 10^{33}$ erg s⁻¹; 20% of the time), and sometimes flares ($L_X \sim 5 \times 10^{34}$ erg s⁻¹, 2%

of the time; Bogdanov et al. 2015, B15 hereafter; Jaodand et al. 2016, J16 hereafter) on a timescale of tens of seconds. Coherent X-ray pulsations assumed to be accretion powered were detected during the high mode (but not in the low mode; Archibald et al. 2015). The optical emission of PSR J1023+0038 in the disk state ($g \simeq 16.5$ mag) became one magnitude brighter than in the radio pulsar state ($g \simeq 17.5$), and was dominated by the reprocessing of the X-ray emission from the disk and the illuminated face of the donor (Coti Zelati et al. 2014, CZ14 hereafter). Flares were also observed in the optical band (Bond et al. 2002, B15) and sometimes also a mode switching similar to that observed in X-rays (Shahbaz et al. 2015, S15 henceforth). Optical pulsations with an amplitude of less than 1% were also detected; even if observed when the source had a disk, they could be hardly reconciled with accretion and it has been suggested that a rotation-powered pulsar might be operating (Ambrosino et al. 2017). In this Letter we present an extensive optical monitoring performed with the NASA *Kepler* Space Telescope when the source was in its current subluminescent accretion disk state.

2. K2 Observations, Analysis, and Results

PSR J1023+0038 was observed by the *K2* mission during campaign 14 between 2017 June 01 05:21:11 UT and 2017 August 19 21:56:19 UT (see Figure 1). Here we analyze short-cadence (SC) data (cadence of 58.8 s) obtained from the Mikulski Archive for Space Telescope (MAST) archive. The

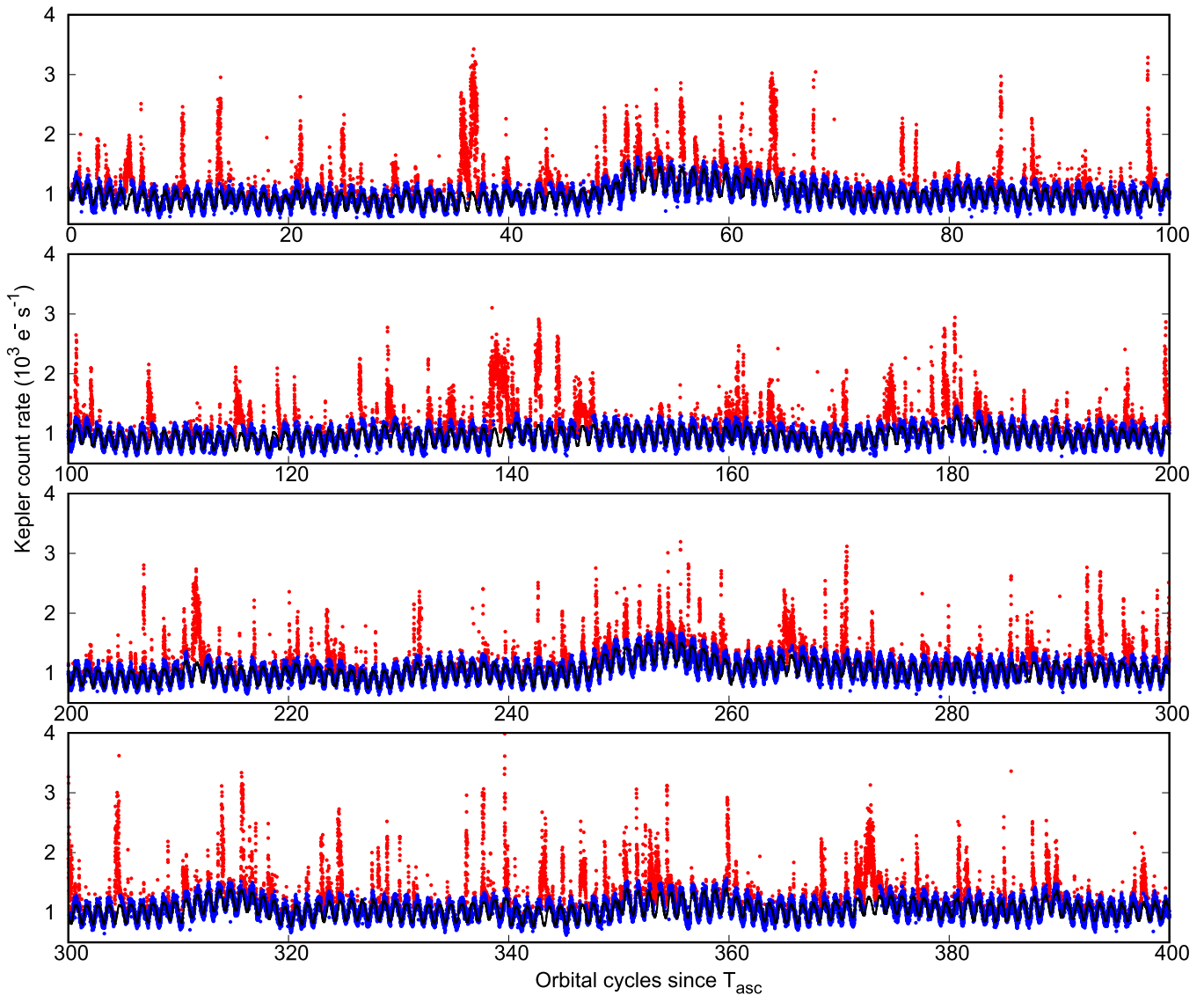


Figure 1. PSR J1023+0038 optical light curve observed by *K2*. Time is expressed in orbital cycles since $T_{\text{asc}} = 57905.1493086$ MJD, assuming $P_{\text{orb}} = 17115.5216592$ s (Jaodand et al. 2016; A. Papitto et al. 2018, in preparation). Flares are plotted with red dots, while the non-flaring emission is plotted using blue dots. The black solid line is the best-fitting model of the non-flaring emission (see the text for details).

data is provided in raw format, consisting of target pixel data. For each 58.8 s exposure we have an 8×8 pixel image centered on the target. PSR J1023+0038 was near the edge of module 16.4. Although this module is not known to be affected by Moiré Pattern Drift noise, the target point-spread function (PSF) is asymmetric as it lies at the edge of one of the outermost modules. As no other sources are known to exist within the 8×8 pixel images, we created the light curve by manually defining a large target mask as well as a background mask. A large target mask is required due to occasional small-scale jittering of the spacecraft, resulting in the target moving slightly from its nominal position, as well as including the elongated PSF of PSR J1023+0038. The inset in the lower-left corner of Figure 2 shows the average masks obtained from 117,030 individual target images, as well as the background pixels used. We removed 1691 observations because of bad quality due to occasional spacecraft rolls or cosmic rays. Figure 2 also shows the target and background masks in red and black, respectively. We produced the light curve by summing together all of the target pixels for each exposure, and

subtracted the average background. The photometric time series was then converted to the solar system barycenter.

To convert *Kepler* flux to magnitudes, we considered two *Hubble Space Telescope Space Telescope Imaging Spectrograph* (*HST* STIS)/charge-coupled device (CCD) 1-s unfiltered acquisition images taken on 2017 June 13 and available on the MAST archive. Assuming the same spectral energy distribution observed in 2014 (see Figure 4.3 of Hernandez Santisteban 2016), the *HST* count rate translates into magnitudes of $g = 16.47(4)$ and $r = 16.48(4)$ mag. The average flux observed by *Kepler* during the 1-minute intervals overlapping with *HST* observations was $S_0 = 1323(5) e^- s^{-1}$; using the relation given by Brown et al. (2011) to estimate the *Kepler* magnitude as $K_p = 0.1g + 0.9r$ for $(g - r) \leq 0.8$, we obtained the conversion $K_p = 16.48 - 2.5 \log(S/S_0)$, where S is the *Kepler* flux in $e^- s^{-1}$. Variability on timescales shorter than the *Kepler* time resolution and flux-dependent color changes both introduce an uncertainty by ~ 0.1 mag.

The *Kepler* light curve is highly variable ($\langle S \rangle = 1083 e^- s^{-1}$, $S_{\text{rms}} = 286 e^- s^{-1}$; Figure 1), reaching up to $3950 e^- s^{-1}$ (i.e.,

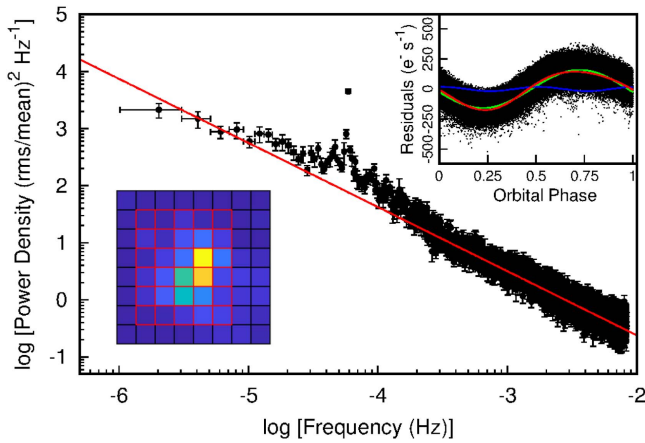


Figure 2. Power-density spectrum obtained averaging 15 intervals, each 3 days long, and normalized to give the squared rms fractional variability. The red line shows a power-law function $P(\nu) \propto \nu^\beta$, with $\beta = -1.12 \pm 0.01$. The inset in the lower-left corner shows the K2 average target pixel image for PSR J1023+0038. The target mask pixels are marked in red, while background mask pixels are marked in black. The inset in the upper-right corner shows the residual light curve folded at the 4.75 hr orbital period, after removing the flares and the long-term trend evaluated with a quadratic function over two-day intervals. The red solid line shows the best-fitting two-harmonic decomposition, the green and the blue solid lines show the first and the second harmonic, respectively.

$K_p \simeq 15.3$ mag). We identified: (i) flares lasting from minutes up to ~ 14 hr, (ii) a periodic modulation at the 4.75 hr binary orbital period, and (iii) a variation of the average optical luminosity over a timescale of days. Figure 2 shows the power-density spectrum calculated averaging three-day intervals, and normalized to the fractional rms amplitude per unit frequency. The spectrum is approximately described by a power law $P(\nu) \propto \nu^\beta$ with $\beta = -1.12 \pm 0.01$ (errors are given at $1\text{-}\sigma$ confidence level throughout the Letter), similar to the value found by S15, above which an excess peaking at the orbital frequency is evident (see Figure 2).

2.1. Flaring Orbital Variability

In order to study the flare characteristics, we first isolated them from the lower-amplitude variations. To this aim we divided the K2 light curve into 41 intervals each spanning 10 orbital cycles (i.e., $\simeq 2$ days), and fitted the count rate with a function consisting of the sum of a quadratic polynomial function and a Fourier decomposition with period $P_{\text{orb}} = 17115.5216592$ s (J16). In some of the intervals up to seven harmonic components were detected, while two were enough in most of the cases. We modeled with a Gaussian function the negative portion of the distribution of light curve residuals with respect to the best-fitting function, and identified as flares the 58.8-s bins found above 3σ the Gaussian median value. Only the negative portion of the histogram was considered to model the non-flaring flux distribution, as the positive end is clearly contaminated by flares. Flares were then removed from the light curve and the fitting procedure iterated until no further flares were identified from the residuals. Figure 3 shows the final residuals histogram; time intervals with a residuals larger than $\simeq 165 e^- s^{-1}$ were deemed as flares. On average the source flared for 15.6% of the time covered by our K2 observations, a fraction variable between 6% and 30% over \simeq two-day intervals. We fitted the 149 brightest flares with a Gaussian profile determining the FWHM, time of maximum, and

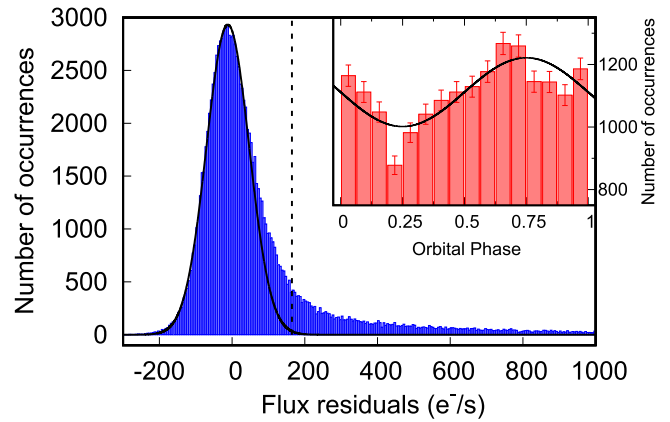


Figure 3. Distribution of the flux residuals in $e^- s^{-1}$ with respect to the best-fitting function (see the text for details), calculated over $\Delta t = 58.8$ -s time bins. The solid line represents the best-fitting Gaussian of the negative portion of the distribution. The dashed vertical line marks the threshold above which the source was identified as flaring. The inset shows the orbital phase distribution of the flare interval. Zero orbital phase corresponds to the passage of the pulsar at the ascending node of the orbit. The best-fitting sinusoid with orbital period and phase fixed to the values derived from X-ray pulsar timing analysis is plotted as a black solid line. Maximum occurs at orbital phase 0.75, i.e., when the donor star is at superior conjunction.

intensity. Flares appear of impulsive nature. They typically lasted less than one hour, with a distribution peaking around 45 minutes and with amplitudes spanning from 0.2 to 1 mag and no clear correlation between duration and amplitude. When short they have a quasi-Gaussian shape, while the longer ones appear to be made up by trains of short impulsive flares.

To study the orbital phase dependence of the flares, we evaluated the orbital phase of each flaring time bin using the epoch of passage of the pulsar at the ascending node determined from the X-ray pulsations detected in the *XMM-Newton* observations performed on 2017 May 23 and 24, $T_{\text{asc}} = 57896.8292633(2)$ MJD (A. Papitto et al. 2018, in preparation) as the zero phase reference. Note that in these units the inferior conjunction of the donor star takes place at phase 0.25. The flare orbital phase histogram has a maximum around phase 0.75 (see the inset of Figure 3), i.e., when the donor star is at superior conjunction. The fractional amplitude evaluated from a sinusoid with fixed period and phase is $A = (9.9 \pm 2.0)\%$. We note that the bin time adopted to study the orbital dependence of flare occurrence is such that the longest flares weighted more in the overall phase distribution.

2.2. Non-flaring Orbital Variability

A bimodality of the non-flaring emission between a high and a low mode each lasting for tens of minutes, similar to that observed in X-rays (B15) and reported in the optical band by S15 (compare their Figure 4), appeared neither in the histogram of residuals calculated over the whole K2 exposure (Figure 3) nor those ranging over 2 -day intervals. Restricting the analysis to two orbital cycles, hints of a bimodality appeared in a dozen out of the 200 intervals considered, even if sharp-edged rectangular dips could be hardly detected in the residual light curve. In those intervals, the low mode occurred more frequently than the high one, similar to what was found by S15 and opposite with respect to the X-ray behavior. Figure 4 shows the trend of the non-flaring flux evaluated as the average value of the quadratic function used in fitting time intervals spanning $\simeq 2$ days, the fractional amplitude, and the phase of

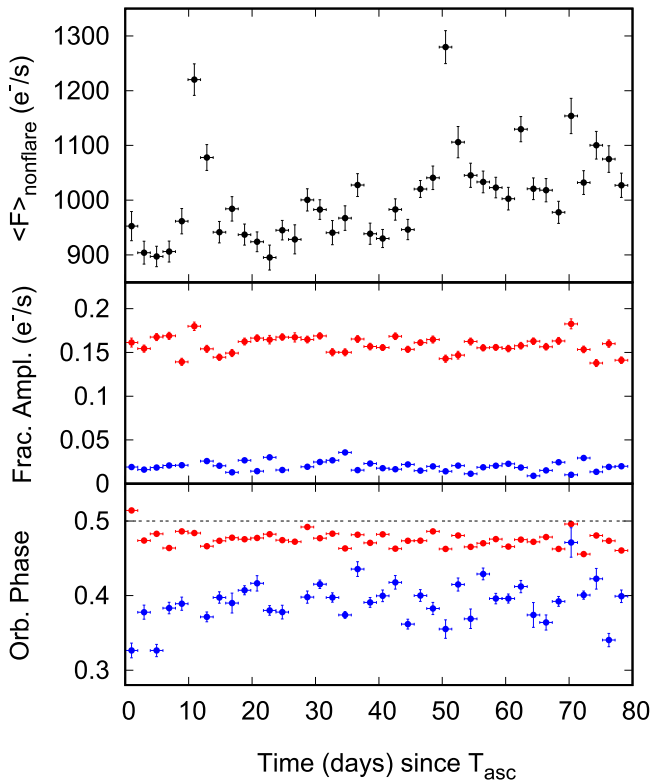


Figure 4. Non-flaring average flux evaluated as the mean of the quadratic function used in fitting time intervals of the *Kepler* light curve spanning 10 orbital cycles (i.e., 47.5 hr, top panel). Fractional amplitude of the first (red dots) and second (blue dots) harmonic of the modulation at the orbital period of the system (middle panel). Phase of the first (red dots) and second (blue dots) harmonic with respect to the epoch of passage of the pulsar at the ascending node according to the X-ray pulsar timing solution (bottom panel).

the first and second harmonic employed to fit the orbital modulation. The average non-flaring flux was clearly variable. Four episodes of brightening can be identified, with count rate increasing by up to 40% on a timescale of $\simeq 4$ days. There was no correlation between the average non-flaring flux and the total fluence of flares. The two peaks at ≈ 10 and ≈ 50 days since T_{asc} might hint at a super-orbital variability, but the interval covered by the *K2* data is too short to assess that. The fractional amplitude of the first and second harmonics used to model the orbital modulation are variable by a few percent around an average value of $\langle A_1 \rangle = 15.9 \pm 0.1\%$ and $\langle A_2 \rangle = 1.8 \pm 0.1\%$, respectively. The average phases of the first and second harmonic are $\langle \phi_1 \rangle = 0.476(2)$ and $\langle \phi_2 \rangle = 0.393(4)$, respectively; as a consequence, the maximum of the sinusoidal modulation takes place on average at phase $\langle \phi_{\text{max}} \rangle = 0.698$ (with a standard deviation of 0.031), 890 ± 85 s earlier than the donor superior conjunction. The average orbital modulation is plotted in the inset in the upper-right corner of Figure 2 as the light curve residuals folded at the 4.75 hr orbital period, after removing the flares and the long-term trend evaluated with a quadratic function over 2-day intervals.

3. Discussion

The multiwavelength phenomenology of the transitional millisecond pulsar PSR J1023+0038 in the subluminal accretion disk state is extremely complex. Variable emission on timescales ranging from millisecond to years was observed

from the radio up to the gamma-ray energy bands. The analysis of the uninterrupted *K2* light curve presented here gives an unprecedented view of its optical variability from minutes to 80 days.

More than 170 optical flares were observed (i.e., $\simeq 2 \text{ day}^{-1}$), both short (\sim minutes) and long (up to ~ 14 hr), with no significant correlation between the duration and the amplitude. The brightest flares attained $K_p = 15.3$ mag, i.e., $\simeq 1.25$ mag brighter than the non-flaring emission. While small samples of optical flares with similar properties have been already reported by Bond et al. (2002), B15, S16, and Hakala & Kajava (2018, HK18 hereafter), the long uninterrupted *Kepler* coverage allowed us to determine for the first time that on average the source was flaring 15.6% of the time, with a flare occurrence of 20% higher at orbital phases corresponding to the donor superior conjunction.

Flares from PSR J1023+0038 were observed simultaneously in the X-ray, UV, optical, and near-infrared (NIR) bands, suggesting they are related to the same process (B15, HK18), with most of the energy released at X-ray energies ($L_X \simeq 6 \times 10^{34} \text{ erg s}^{-1}$, $L_X/L_{\text{opt}} \simeq 6$). We compare the fraction of the *K2* light curve characterized by optical flares to that observed in the X-ray band, where PSR J1023+0038 has been intensively observed. The *Swift* satellite observed PSR J1023+0038 for 30 times simultaneously with the *Kepler* campaign, for a total on-source time of ~ 1.1 days, but the relatively low photon statistics of the *Swift* X-Ray Telescope only allowed us to identify clearly one X-ray flare associated with an optical flare. On the other hand, PSR J1023+0038 was observed 10 times by *XMM-Newton* for a total exposure of 5.6 days between 2013 June and 2015 December (Archibald et al. 2015, B15, J16). The source spent $\simeq 2\%$ of the time flaring in X-rays (J16), less than the flaring-time fraction observed by *K2* even taking into account its variability over 2-day intervals (values as low as 6% were observed). Only part of this discrepancy can be ascribed to the lower count rate recorded by *XMM-Newton* with respect to *Kepler*. X-ray flares were in fact identified by *XMM-Newton* when the ratio between the 0.5 and 10 keV net flare count rate and that observed in the high mode was larger than $(S_{\text{flare,min}}/S_{\text{high}})_{\text{Xray}} \simeq 11/7-1 \simeq 0.6$ (B15). For the brightest flares, the ratio ξ between the flare and non-flaring flux observed in the optical ($(S_{\text{flare}}/S)_{\text{opt}} \simeq 4000/1000 - 1 \simeq 3$), and in the X-ray band ($(S_{\text{flare,max}}/S_{\text{high}})_{\text{Xray}} \simeq 60/7-1 \simeq 7.5$, see e.g., Figure 7 in J16) was $\xi \simeq 3/7.5 = 0.4$. Assuming that this ratio held for all flares—a conservative hypothesis as not all the X-ray flares have an optical counterpart—we conclude that the fainter flares detectable by *XMM-Newton* would have a residual *Kepler* flux of $\xi \times (S_{\text{flare,min}}/S_{\text{high}})_{\text{Xray}} \times \langle S \rangle_{\text{Kep}} \simeq 260 \text{ e}^- \text{ s}^{-1}$. The fraction of time spent by PSR J1023+0038 during *K2* observations above such a threshold is 10.3%. We conclude that even taking into account variability on intervals of a few days and the difference in the sensitivity of *Kepler* and *XMM-Newton*, the observed flaring-time fraction observed by *Kepler* can be taken as an indication that the source spent a larger portion of the time flaring in 2017 June/July than in 2013–2015. It is not clear what may have caused such an increase, as the X-ray properties observed by *Swift* simultaneously to the *K2* campaign 14 and during *XMM-Newton* observations performed on 2017 May 23 and 24, i.e., just before it, were consistent with those determined during previous years.

Our analysis showed that optical flares were seen close to the donor superior conjunction more often, whereas no dependence of the X-ray flare detection on the orbital phase has yet been reported, possibly because only a handful of X-ray flares have been actually observed so far. Note that, however, after this Letter was submitted we became aware of an analysis of the same *K2* data set by Kennedy et al. (2018), who used a slightly different algorithm to define flares. According to their definition flares occurred more often than from our analysis (22% of the time) and the flare peaks did not show a significant dependence on the orbital phase. We then conclude that the orbital dependence of flares is uncertain and heavily depends on their definition. If confirmed, a dependence of the optical flares observation rate on the orbital phase would indicate that at least part of the flares originated from reprocessing of the X-ray emission off the surface of the companion star. However, the spectral colors observed by S15 from one bright optical flare indicated that it originated in an optically thin medium such an accretion disk corona and/or hot fireball ejecta. These could be launched by a propelling magnetosphere (Papitto et al. 2014; Papitto & Torres 2015), or by the wind of a rotation-powered pulsar assumed to be active in spite of the presence of an accretion disk (Takata et al. 2014, CZ14, Ambrosino et al. 2017). In the latter case, flares could be produced by the interaction of a relativistic pulsar wind with clumps of matter in the region beyond the light cylinder (see, e.g., Zdziarski et al. 2010). A change of the accretion flow during flares possibly related to absorption by ejecta of matter is also supported by the lack of H_α emission from the portion of the disk that is closest to the observer in between orbital phases 0.25–0.5, and by the appearance of an additional polarized emission (HK18; see also Baglio et al. 2016). Assuming that flares originated from the ejecta, an orbital dependence could indicate that matter is preferentially launched from a spot in the disk along the line that joins the pulsar and the donor star, possibly close to the inner Lagrangian point. A similar scenario was put forward by de Martino et al. (2014) to explain the disappearance of emission lines that had originated in the outer disk regions of the transitional MSP XSS J12270–4859, when the donor was at its superior conjunction.

The first and second harmonics of the Fourier decomposition used to model the orbital modulation had an average fractional amplitude of $\simeq 15.9$ and $\simeq 1.8\%$, respectively. Generally, the first harmonic is ascribed to irradiation of the companion star by the X-ray source with an expected maximum close to the donor superior conjunction, while the second is assumed to trace the ellipsoidal deformation of the companion star and has maxima when the donor is at quadrature. On average, the observed orbital modulation had a maximum that preceded the donor superior conjunction by 890 ± 85 s. Assuming that most of the orbital modulation arises from the vicinity of the inner Lagrangian point, and taking $M_1 = 1.4 M_\odot$ and $M_2 = 0.2 M_\odot$ for the mass of the primary and the donor, respectively, this lag translates into an arc-length of $\simeq 2.5 \times 10^9$ cm, which is smaller than the radius of the donor star ($R_2 \simeq 3 \times 10^{10}$ cm). A number of effects can produce the observed lags between the phase of the first harmonic of the optical orbital modulation and the donor superior conjunction; namely (i) asymmetric heating of the companion due to screening of irradiating X-rays by intervening material such as matter ejected from the disk, (ii) a contribution from matter streaming past the inner Lagrangian point, and (iii) absorption of the companion star emission by

the ejecta launched from the vicinity of the inner Lagrangian point.



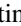

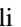


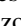

The average non-flaring optical emission varied by up to 40% over timescales of a few days during the *K2* campaign, ranging from $K_p = 16.9$ to 16.5. In comparison, the average flux reported by CZ14 corresponds to a *K2* magnitude of $K_p = 16.36(2)$. Similar large variations of the X-ray flux were not observed in past observations, nor in the *Swift* monitoring during the *Kepler* observations. B15 reported that the X-ray flux observed in the high mode (in which the source spends $\sim 70\%$ of the time) decreased by just a few percent between 2013 November and 2014 June. In addition, the X-ray flux observed in the high and *low* mode during *XMM-Newton* observations performed one week before the start of the *K2* campaign was still consistent with that determined by B15 about three years earlier. We did not find a correlation between the optical flare fluence (possibly related to the fluence of the X-ray flares) and the average non-flaring optical emission. The observed variations of the non-flaring optical emission could be then due to variability of the outer disk intrinsic emission caused by variations in the mass inflow rate that would not be reflected by a concurrent increase in the X-ray emission, possibly because of mass ejection before the mass gets close enough to the NS to emit high-energy radiation. Alternatively, changes in the angle subtended by the medium that reprocesses high-energy radiation into visible emission could have occurred, suggesting a very complex and variable geometry of the accretion flow between the inner Lagrangian point and the outer disk regions, and/or azimuthal extent changes of the latter.

Finally, we note that hints for a bimodal flux distribution like those reported at some epochs by S15 appeared only in a dozen two-orbital-cycle intervals (i.e., $\sim 8\%$ of the total) of the *K2* data that we analyzed. Optical dips were not detected at other epochs (J16, HK18), indicating that these features are not stable as in the X-ray band. When observed (S15), dips had ingress/egress times of 12–35 s, duration in the range 80–1300 s, and a separation of 200–1900 s. These properties are similar to those of the *low* mode dips observed in the X-ray band for $\sim 20\%$ of the time (B15, J16), and were claimed to be their equivalent, even if simultaneous observations were lacking. Note that when a bimodal distribution of the optical flux is observed (S15, or in a few intervals of the *K2* data analyzed here, the low flux mode is predominant, whereas the opposite happens in the X-rays. The time resolution (~ 60 s) of *K2* data could well cause smearing of the sharp ingress/egress shape of the dips, but should not have prevented the detection of the long (20-minute) dips interleaved by less than an hour. Even when a bimodality of the flux was suggested by the residual flux distribution, the light curve did not show such prolonged dips. Future simultaneous optical and X-ray monitoring will possibly ascertain whether the lack of optical dips marked a change in the properties of the source.

A.P. acknowledges funding from the EU’s Horizon 2020 Framework Programme for Research and Innovation under the Marie Skłodowska-Curie Individual Fellowship grant agreement 660657-TMSP-H2020-MSCA-IF-2014, and from the agreements ASI-INAF I/037/12/0 and ASI-INAF 2017-14-H.O. N.R., F.C.Z., and D.F.T. acknowledge funding from grants AYA2015-71042-P and SGR 2017-1383.

A.S. acknowledges funding from grants ESP2017-82674-R (MINECO) and 2017-SGR-1131.

ORCID iDs

A. Papitto  <https://orcid.org/0000-0001-6289-7413>
 N. Rea  <https://orcid.org/0000-0003-2177-6388>
 D. de Martino  <https://orcid.org/0000-0002-5069-4202>
 S. Campana  <https://orcid.org/0000-0001-6278-1576>
 A. Serenelli  <https://orcid.org/0000-0001-6359-2769>
 L. Stella  <https://orcid.org/0000-0002-0018-1687>
 D. F. Torres  <https://orcid.org/0000-0002-1522-9065>
 P. D'Avanzo  <https://orcid.org/0000-0001-7164-1508>
 G. L. Israel  <https://orcid.org/0000-0001-5480-6438>

References

- Ambrosino, F., Papitto, A., Stella, L., et al. 2017, *NatAs*, **1**, 854
 Archibald, A. M., Bogdanov, S., Patruno, A., et al. 2015, *ApJ*, **807**, 62
 Archibald, A. M., Stairs, I. H., Ransom, S. M., et al. 2009, *Sci*, **324**, 1411
 Baglio, M. C., D'Avanzo, P., Campana, S., et al. 2016, *A&A*, **591**, A101
 Bassa, C. G., Patruno, A., Hessels, J. W. T., et al. 2014, *MNRAS*, **441**, 1825
 Bogdanov, S., Archibald, A. M., Bassa, C., et al. 2015, *ApJ*, **806**, 148
 Bond, H. E., White, R. L., Becker, R. H., & O'Brien, M. S. 2002, *PASP*, **114**, 1359
 Brown, T. M., Latham, D. W., Everett, M. E., & Esquerdo, G. A. 2011, *AJ*, **142**, 112
 Coti Zelati, F., Baglio, M. C., Campana, S., et al. 2014, *MNRAS*, **444**, 1783
 de Martino, D., Casares, J., Mason, E., et al. 2014, *MNRAS*, **444**, 3004
 de Martino, D., Falanga, M., Bonnet-Bidaud, J.-M., et al. 2010, *A&A*, **515**, A25
 Hakala, P., & Kajava, J. J. E. 2018, *MNRAS*, **474**, 3297
 Halpern, J. P., Gaidos, E., Sheffield, A., Price-Whelan, A. M., & Bogdanov, S. 2013, *ATel*, **5514**, 1
 Hernandez Santisteban, J. V. 2016, PhD thesis, Univ. Southampton
 Jaodand, A., Archibald, A. M., Hessels, J. W. T., et al. 2016, *ApJ*, **830**, 122
 Kennedy, M. R., Clark, C. J., Voisin, G., & Breton, R. 2018, *MNRAS*, **477**, 1120
 Papitto, A., Ferrigno, C., Bozzo, E., et al. 2013, *Natur*, **501**, 517
 Papitto, A., & Torres, D. F. 2015, *ApJ*, **807**, 33
 Papitto, A., Torres, D. F., & Li, J. 2014, *MNRAS*, **438**, 2105
 Patruno, A., Archibald, A. M., Hessels, J. W. T., et al. 2014, *ApJL*, **781**, L3
 Shahbaz, T., Linares, M., Nevado, S. P., et al. 2015, *MNRAS*, **453**, 3461
 Stappers, B. W., Archibald, A. M., Hessels, J. W. T., et al. 2014, *ApJ*, **790**, 39
 Takata, J., Li, K. L., Leung, G. C. K., et al. 2014, *ApJ*, **785**, 131
 Tendulkar, S. P., Yang, C., An, H., et al. 2014, *ApJ*, **791**, 77
 Torres, D. F., Ji, L., Li, J., et al. 2017, *ApJ*, **836**, 68
 Zdziarski, A. A., Neronov, A., & Chernyakova, M. 2010, *MNRAS*, **403**, 1873